Plasmon-enhanced emission from optically-doped MOS light sources

Aaron C. Hryciw, Young Chul Jun, and Mark L. Brongersma

Geballe Laboratory for Advanced Materials, Stanford University
476 Lomita Mall, Stanford, CA, 94305, U.S.A.

Brongersma@stanford.edu

Abstract: We evaluate the spontaneous emission rate (Purcell) enhancement for optically-doped metal–dielectric–semiconductor light-emitting structures by considering the behavior of a semiclassical oscillating point dipole placed within the dielectric layer. For a Ag–SiO_2–Si structure containing emitters at the center of a 20-nm-thick SiO_2 layer, spontaneous emission rate enhancements of 40 to 60 can be reached in the wavelength range of 600 to 1800 nm, far away from the surface plasmon resonance; similar enhancements are also possible if Al is used instead of Ag. For dipoles contained in the thin oxide layer of a Ag–SiO_2–Si–SiO_2 structure, the emission exhibits strong preferential coupling to a single well-defined Si waveguide mode. This work suggests a means of designing a new class of power-efficient, high-modulation-speed, CMOS-compatible optical sources that take full advantage of the excellent electrical properties and plasmon-enhanced optical properties afforded by MOS devices.

© 2008 Optical Society of America

OCIS codes: (250.5403) Plasmonics; (130.0250) Optoelectronics; (160.3900) Materials: metals; (160.6000) Materials: semiconductor materials; (240.6680) Optics at surfaces: surface plasmons; (230.6080) Sources.

References and links

1. B. Jalali and S. Fathpour, "Silicon photonics," J. Lightwave Tech. **24**, 4600–4615 (2006).
2. M. Lipson, "Guiding, modulating, and emitting light on silicon—Challenges and opportunities," J. Lightwave Tech. **23**, 4222–4238 (2005).
3. L. Pavesi, "Will silicon be the photonic material of the third millenium?" J. Phys. Condens. Matter **15**, R1169–R1196 (2003).
4. L. Pavesi, L. Dal Negro, C. Mazzoleni, G. Franzò, and F. Priolo, "Optical gain in silicon nanocrystals," Nature **408**, 440–444 (2000).
5. A. W. Fang, H. Park, O. Cohen, R. Jones, M. J. Paniccia, and J. E. Bowers, "Electrically pumped hybrid AlGaInAs–silicon evanescent laser," Opt. Express **14**, 9203–9210 (2006).
6. G. W. Ford and W. H. Weber, "Electromagnetic interactions of molecules with metal surfaces," Phys. Rep. **113**, 195–287 (1984).
7. W. L. Barnes, "Electromagnetic crystals for surface plasmon polaritons and the extraction of light from emissive devices," J. Lightwave Tech. **17**, 2170–2182 (1999).
8. J. Vučković, M. Loncar, and A. Scherer, "Surface plasmon enhanced light-emitting diode," IEEE J. Quantum Electron. **36**, 1131–1144 (2000).
9. J. S. Q. Liu and M. Brongersma, "Omnidirectional light emission via surface plasmon polaritons," Appl. Phys. Lett. **90**, 091116 (2007).
10. Y. C. Jun, R. D. Kekatpure, J. S. White, and M. Brongersma, "Nonresonant enhancement of spontaneous emission in metal–dielectric–metal plasmon waveguide structures," Phys. Rev. B **78**, 153111 (2008).
11. S. Wang, A. Eckau, E. Neufeld, R. Carius, and C. Buchal, "Hot electron impact excitation cross-section of Er^{3+} and electroluminescence from erbium-implanted silicon metal-oxide-semiconductor tunnel diodes," Appl. Phys. Lett. **71**, 2824–2826 (1997).

#102844 - $15.00 USD Received 16 Oct 2008; revised 19 Dec 2008; accepted 22 Dec 2008; published 24 Dec 2008

12. K. Sun, W. J. Xu, B. Zhang, L. P. You, G. Z. Ran, and G. G. Qin, "Strong enhancement of Er^{3+} 1.54 μm electroluminescence through amorphous Si nanoparticles," Nanotechnology **19**, 105,708 (2008).
13. A. Irrera, D. Pacifici, M. Miritello, G. Franzò, F. Priolo, F. Iacona, D. Sanfillipo, G. Di Stefano, and P. G. Fallica, "Electroluminescence properties of light emitting devices based on silicon nanocrystals," Physica E **16**, 395–399 (2003).
14. P. Yeh, *Optical waves in layered media*, 2nd ed. (Wiley-Interscience, New York, 2005).
15. A. D. Rakić, A. B. Djurišić, J. M. Elazar, and M. L. Majewski, "Optical properties of metallic films for vertical-cavity optoelectronic devices," Appl. Opt. **37**, 5271–2383 (1998).
16. D. R. Lide, ed., *CRC Handbook of Chemistry and Physics, Internet Version 2008*, 88th ed. (Taylor & Francis, Boca Raton, FL, 2008).
17. J. J. Burke, G. I. Stegeman, and T. Tamir, "Surface-polariton-like waves guided by thin, lossy metal films," Phys. Rev. B **33**, 5186–5201 (1986).
18. G. T. Reed and A. P. Knights, *Silicon photonics: an introduction* (John Wiley and Sons, Ltd., Chichester, England, 2004).
19. R. J. Walters, J. Kalkman, A. Polman, H. A. Atwater, and M. J. A. de Dood, "Photoluminescence quantum efficiency of dense silicon nanocrystal ensembles in SiO_2," Phys. Rev. B **73**, 132302 (2006).
20. K. S. Cho, N. M. Park, T. Y. Kim, K. H. Kim, G. Y. Sung, and J. H. Shin, "High efficiency visible electroluminescence from silicon nanocrystals embedded in silicon nitride using a transparent doping layer", Appl. Phys. Lett. **86**, 071909 (2005).

1. Introduction

A host of diverse applications, from optical computing to telecommunications to biosensing, will be enabled once silicon-based photonics is wedded monolithically to electronics [1]. Although there has been tremendous progress with respect to Si-based photonic components such as waveguides, modulators, and detectors [1, 2, 3], the persistent absence of an efficient, high-modulation-frequency, CMOS-compatible, on-chip light source has thus far prevented researchers from attaining this Holy Grail. An intense worldwide research effort toward a Si-based laser has been ongoing since the early 1990s, but despite a report of net optical gain in Si nanocrystals [4], Si photonic chips still must rely on external lasers ("photonic batteries") [1, 3] or wafer-bonded III–V lasers [5]. This lack of success can in part be traced to the slow decay rate and concomitant low gain cross-sections of the most popular Si-compatible emitters (e.g., rare-earth ions and Si nanostructures in SiO_2). Moreover, light sources exhibit a large mismatch between electronic and photonic length scales: from an electronics viewpoint, thin devices are desirable for effective charge injection at low bias, while from a photonics viewpoint, thicker devices are preferred to increase mode overlap with the active, light-emitting region. It is therefore of great interest to consider phenomena which can enhance the light-emission process in thin optical structures congruent with CMOS electronics.

As a key building-block of the integrated electronics industry, the metal–oxide–semiconductor (MOS) structure is fabricated using mature Si processing technology and has been studied exhaustively with respect to its electrical properties. In stark contrast, its optical properties have largely been ignored, as the top metal gate is generally considered too reflective or absorbing for optical applications. Interestingly, it is well documented that an increase in the spontaneous emission decay rate of dipolar emitters, such as fluorescent molecules or quantum dots, can be attained by placing them near metal surfaces [6]. When close to the metal surface, new decay pathways open up for the emitter, including decay into surface plasmon-polariton (SPP) modes. SPPs are electron density waves propagating along metal–dielectric interfaces which exhibit a strong coupling to electromagnetic fields ("light"). In conventional solid-state lighting devices, the excitation of SPPs is suppressed as much as possible: the SPP energy is typically dissipated in the metal, lowering device efficiency.

Recently, several attempts have been made to recover the energy coupled to SPPs by using nanostructured metals in light-emitting devices. This can increase the out-coupling efficiency, decrease the radiative lifetime of emitters, and modify the angular distribution of the emission

#102844 - $15.00 USD Received 16 Oct 2008; revised 19 Dec 2008; accepted 22 Dec 2008; published 24 Dec 2008
(C) 2009 OSA

[7, 8, 9]. Particularly pronounced changes in decay rates were recently predicted for metal–dielectric–metal (MDM) waveguides that support highly confined SPP modes [10]. The high dielectric contrast between the different layers in MOS structures also gives rise to highly-confined transverse magnetic (TM) modes; this is a direct consequence of the required continuity of the normal component of the dielectric displacement, $D_{\mathrm{n}} = \varepsilon E_{\mathrm{n}}$, at any interface. Large increases in the decay rate of emitters embedded in the low-index oxide can thus be expected in these structures as well. The possibility to realize optically-doped MOS sources on Si may have tremendous potential based on ease of fabrication. Furthermore, efficient coupling to Si waveguides is straightforward if such sources are realized using silicon-on-insulator (SOI) technology. A schematic of a simple, on-chip light source applying this principle is shown in Fig. 1. This figure clearly shows the enhanced fields inside the oxide for a single supported TM mode and illustrates the possibility of coupling to a SOI waveguide. Although light sources based on MOS structures containing erbium [11, 12] or Si nanocrystals [13] in the oxide layer have been demonstrated, the reports have focused on the electrical behavior of the devices; to the authors' knowledge, evaluating metal–dielectric–semiconductor (MDS) light-emitting structures for decay rate enhancement has not yet been considered. The design of a device such as shown in Fig. 1 would involve analysis of the spontaneous emission rate enhancement, mode-coupling efficiencies, and charge-carrier injection; in this paper, we focus only on the first of these aspects.

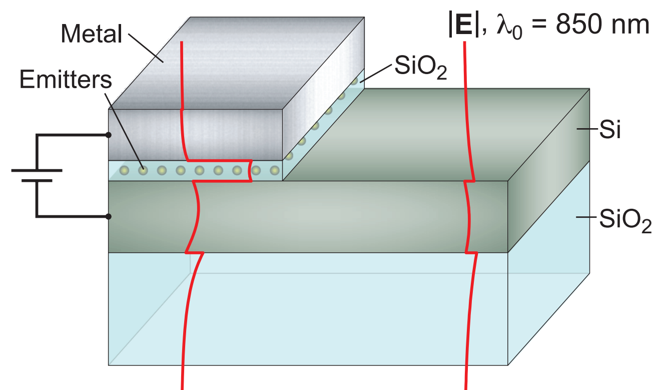

Fig. 1. Schematic of a prototype CMOS-compatible light-emitting device architecture exploiting plasmonic decay rate enhancement of emitters in a planar metal–dielectric–semiconductor–dielectric (MDSD) structure and the possibility of coupling the emission into a SOI waveguide. Typical electric field profiles for supported transverse magnetic (TM) modes are shown in red.

2. Model

We investigate the behavior of an emitter in a MDS structure by considering it as a semiclassical point dipole oscillating with angular frequency ω [6]. In this approximation, the decay rate γ of the dipole is related to its dissipated power $\mathscr{P}$ via $\gamma = \mathscr{P}/\hbar\omega$, where $\hbar$ is Planck's constant divided by 2π. In general, for a dipole in a planar structure, the total electric field $\mathbf{E}$ at its position will comprise both the field emitted away from the dipole as well as the reflected field from the various interfaces. Depending on the phase offset between these fields, the decay rate can be either enhanced or suppressed. As a dipole approaches a metal surface, the decay rate increases rapidly due to desirable coupling to SPP modes and unwanted coupling to absorptive lossy surface waves (LSW) [6]. It is important to note that coupling to a well-defined SPP mode

#102844 - $15.00 USD Received 16 Oct 2008; revised 19 Dec 2008; accepted 22 Dec 2008; published 24 Dec 2008
(C) 2009 OSA

is advantageous, since this energy may later be coupled into useful waveguide modes.

The most general planar geometry we consider is that of a point dipole in a dielectric slab of thickness L_{D} and real dielectric constant ε_{D}, sandwiched between upper and lower claddings consisting of multilayer stacks. For a dipole with internal quantum efficiency η and decay rate γ_{free} in an infinite dielectric, the normalized decay rate in the layered structure may be written as [6]

$$\hat{\gamma} \equiv \frac{\gamma}{\gamma_{\mathrm{free}}} = 1 - \eta + \eta \int_0^\infty \frac{1}{\mathscr{P}_{\mathrm{free}}} \frac{\mathrm{d}\mathscr{P}}{\mathrm{d}k_\parallel} \, \mathrm{d}k_\parallel. \tag{1}$$

When a dipole is oriented at an angle θ from the normal to the interfaces, the integrand in Eq. (1) is given by

$$\frac{1}{\mathscr{P}_{\mathrm{free}}} \frac{\mathrm{d}\mathscr{P}}{\mathrm{d}k_\parallel} = \frac{3}{2} \frac{1}{k_{\mathrm{D}}^3} \Re\mathrm{e} \left\{ \frac{k_\parallel}{q_{\mathrm{D}}} \left[\cos^2\theta \left(k_\parallel^2 \tilde{r}_\perp^{\mathrm{P}} \right) + \frac{1}{2} \sin^2\theta \left(k_{\mathrm{D}}^2 \tilde{r}_\parallel^{\mathrm{S}} + q_{\mathrm{D}}^2 \tilde{r}_\parallel^{\mathrm{P}} \right) \right] \right\} \tag{2}$$

where

$$\tilde{r}_\perp^{\mathrm{P}} = \frac{\left[1 + r_{\mathrm{D}-}^{\mathrm{P}} \exp(2\mathrm{i}q_{\mathrm{D}} d_-)\right] \left[1 + r_{\mathrm{D}+}^{\mathrm{P}} \exp(2\mathrm{i}q_{\mathrm{D}} d_+)\right]}{1 - r_{\mathrm{D}-}^{\mathrm{P}} r_{\mathrm{D}+}^{\mathrm{P}} \exp(2\mathrm{i}q_{\mathrm{D}} L_{\mathrm{D}})} \tag{3a}$$

$$\tilde{r}_\parallel^{\mathrm{S}} = \frac{\left[1 + r_{\mathrm{D}-}^{\mathrm{S}} \exp(2\mathrm{i}q_{\mathrm{D}} d_-)\right] \left[1 + r_{\mathrm{D}+}^{\mathrm{S}} \exp(2\mathrm{i}q_{\mathrm{D}} d_+)\right]}{1 - r_{\mathrm{D}-}^{\mathrm{S}} r_{\mathrm{D}+}^{\mathrm{S}} \exp(2\mathrm{i}q_{\mathrm{D}} L_{\mathrm{D}})} \tag{3b}$$

$$\tilde{r}_\parallel^{\mathrm{P}} = \frac{\left[1 - r_{\mathrm{D}-}^{\mathrm{P}} \exp(2\mathrm{i}q_{\mathrm{D}} d_-)\right] \left[1 - r_{\mathrm{D}+}^{\mathrm{P}} \exp(2\mathrm{i}q_{\mathrm{D}} d_+)\right]}{1 - r_{\mathrm{D}-}^{\mathrm{P}} r_{\mathrm{D}+}^{\mathrm{P}} \exp(2\mathrm{i}q_{\mathrm{D}} L_{\mathrm{D}})} \tag{3c}$$

take into account the multiple reflections at the dielectric slab's surfaces, $k_{\mathrm{D}} = 2\pi\varepsilon_{\mathrm{D}}^{1/2}/\lambda_0$ is the magnitude of the wavevector in the dielectric, $k_\parallel$ is the in-plane wavevector (propagation constant of the mode), and $q_{\mathrm{D}} = (k_{\mathrm{D}}^2 - k_\parallel^2)^{1/2}$ is the perpendicular (out-of-plane) wavevector. In Eqns. (3), $r_{\mathrm{D}+}^{\mathrm{P,S}}$ and $r_{\mathrm{D}-}^{\mathrm{P,S}}$ are the effective P- and S-polarized (TM and TE) reflectivities at the upper and lower dielectric interfaces, respectively. For a dielectric layer clad with semi-infinite layers, $r_{\mathrm{D}+}^{\mathrm{P,S}}$ and $r_{\mathrm{D}-}^{\mathrm{P,S}}$ reduce to the usual Fresnel reflectivities for single planar interfaces; for multilayer claddings, $r_{\mathrm{D}+}^{\mathrm{P,S}}$ and $r_{\mathrm{D}-}^{\mathrm{P,S}}$ may be calculated using the transfer matrix approach [14].

We start by considering an emitter in the center of a dielectric (D) film ($d_+ = d_- = L_{\mathrm{D}}/2$) clad by semi-infinite metal (M) and semiconductor (S) layers with (complex) dielectric constants ε_{M} and ε_{S}, respectively. Initially, we assume that the dipole is oriented perpendicular to the layer interfaces ($\theta = 0$) and has unit quantum efficiency. This dipole couples most strongly to SPPs, which exhibit an electric field distribution that is dominantly perpendicular to the metal surface. While a complete account of the reflection of light from the D–M and D–S boundaries would include nonlocal effects via dielectric constants exhibiting both temporal and spatial dispersion, that is, $\varepsilon = \varepsilon(\omega, \mathbf{k})$, the layers are reasonably well described as *local* media with $\varepsilon = \varepsilon(\omega)$ so long as the dipole–interface distances are larger than $\sim$10 nm [6]. As such, we simulate a dipole in the center of a 20-nm-thick dielectric layer and use tabulated values for ε_{M} (Ag) [15] and ε_{S} (Si) [16]; for simplicity, we choose a dispersionless dielectric with $\varepsilon_{\mathrm{D}} = 2.25$, approximating that of SiO_2. With its low loss in the visible, Ag serves as an exemplar for this discussion; CMOS-compatible metals such as Al exhibit qualitatively very similar behavior, as discussed later in the text.

3. Results and discussion

Calculated using Eq. (2), the normalized decay rate density for the semi-infinite Ag–SiO_2–Si structure discussed above is shown in Fig. 2. The peaks in the decay rate density at each energy

#102844 - $15.00 USD Received 16 Oct 2008; revised 19 Dec 2008; accepted 22 Dec 2008; published 24 Dec 2008
(C) 2009 OSA

trace out the dispersion of the TM magnetic mode that provides the dominant decay pathway (red curve). Approaching Fig. 2 heuristically, the basic physics of the MDS structure becomes apparent. First, the red dispersion curve lies *above* the Si light line for the entire energy range being considered, in contrast to the bound SPP modes found at a single Ag–Si interface [10]. As such, the field profiles correspond to leaky SPP modes, marked by exponentially-growing solutions in the Si substrate; such solutions are physical insofar as they may be regarded as spatial transients, meaningful only for a finite distance in the Si [17]. While the interpretation of field distributions for leaky modes is thus complicated slightly, the limiting behavior of the dispersion relation remains intuitive. For energies near the Ag–SiO_2 surface plasmon energy ($\hbar\omega_{sp}$), the field becomes more concentrated in the dielectric layer than at low energies (see insets): the MDS dispersion relation's asymptotic approach to this value mimics that of the single-interface DM case [6]. At low energies, however, the MDS dispersion relation approaches the Si light line, since, relative to the high-energy case, the field is drawn out of the oxide layer in favor of the Si substrate.

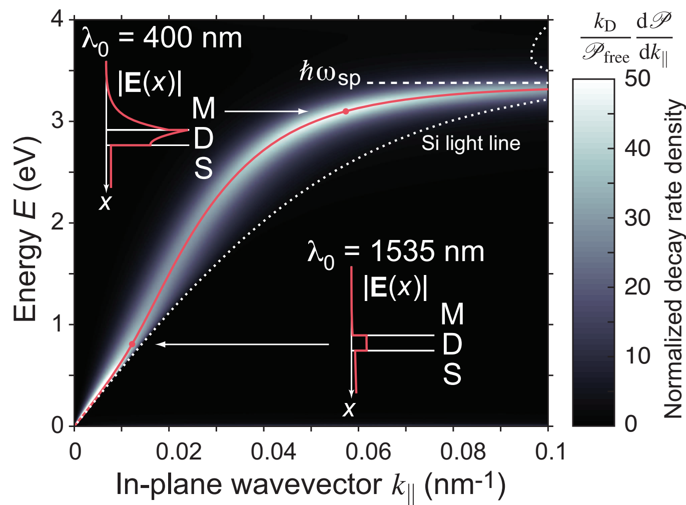

Fig. 2. Normalized decay rate density for a perpendicular dipole located at the center of the 20-nm-thick dielectric layer in a Ag–SiO_2–Si MDS structure. **E**-field profiles, normalized to unit **H**-field magnitude at the M–D interface, are shown in the insets.

The leaky nature of these modes is also highlighted by the difference in the peak width of the normalized decay rate density curves for the MDS and MDM structures, as illustrated in Fig. 3a for an emitter with $\lambda_0 = 1535$ nm. Whereas the MDM case supports a single bound gap-plasmon mode with a relatively well-defined propagation constant [10], the availability of leaky modes in the MDS case broadens its peak considerably. The sharp drop in decay rate density for the MDS plot at the maximum allowable k_{Si} indicates the lack of de-excitation pathways with higher in-plane wavevectors. Decay into such high-$k_{\parallel}$ channels (lossy surface waves) [6], is a purely absorptive loss mechanism, arising from the imaginary part of ε_M.

Although the focus of this paper is on the semi-infinite MDS structure, emission into leaky SPP modes is not useful from the standpoint of on-chip light sources for integrated photonics. We have therefore also included in Fig. 3b the normalized decay rate density for a more viable device architecture (also see Fig. 1). This device structure could be fabricated on SOI, provided that the buried oxide (BOX) layer is sufficiently thick to limit leakage into the Si substrate [18]; in such a case, we may approximate the BOX layer by the infinite dielectric shown in Fig. 3b. In addition to an abrupt shoulder at k_{SiO_2} mark-

#102844 - $15.00 USD Received 16 Oct 2008; revised 19 Dec 2008; accepted 22 Dec 2008; published 24 Dec 2008
(C) 2009 OSA

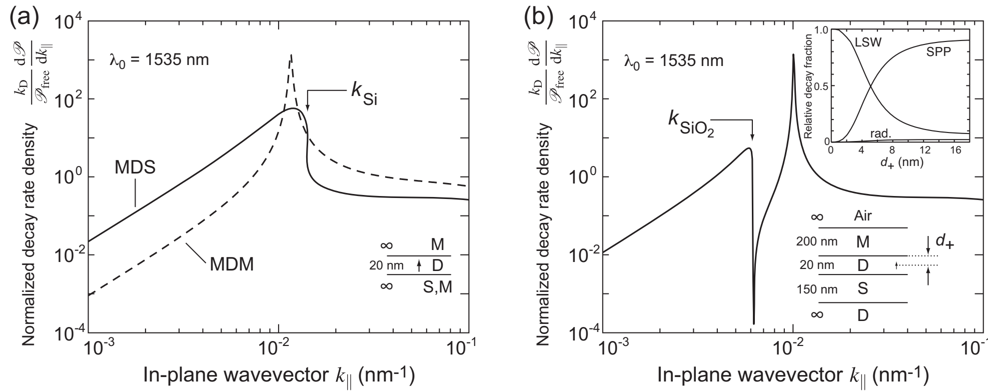

Fig. 3. Decay rate density vs. $k_{\parallel}$ at $\lambda_0 = 1535$ nm and simulation geometries for (a) the semi-infinite MDS and MDM structures, and (b) the MDSD structure; in both cases, the dipole is situated at the center of the dielectric layer. The inset to (b) illustrates the effect of dipole position on the relative contributions of the surface plasmon polariton (SPP), lossy surface wave (LSW), and far-field radiation (rad.) pathways to the overall decay rate in the MDSD structure.

ing the cutoff for SiO_2 radiation modes, the MDSD case exhibits a similar low loss to LSW as in the MDS structure, with a peak of comparable sharpness to the MDM gap-plasmon mode, albeit at lower $k_{\parallel}$; this peak corresponds to a mode with the **E**-field distribution shown on the left side of Fig. 1, and has a propagation of length at 1535 nm of $\sim$20 μm for this geometry.

By integrating over the peak and comparing to the total power emitted by the dipole, we find that roughly 82% is coupled into this mode for a dipole at the center of the dielectric layer. In the inset to Fig. 3b, the efficacy of this coupling as a function of dipole position is illustrated: dipoles closer to the metal couple predominantly to LSWs, with more power being emitted into the MDSD SPP mode as the dipole approaches the Si surface. However, it is important to bear in mind that using a local dielectric constant causes an underestimation of the coupling to LSWs for very small dipole–metal distances ($d_+ < 10$ nm) [6], such that the effect of quenching is likely to be stronger in this regime than predicted in the inset. This demonstrates the importance of careful control over the location of emitters during the fabrication of devices based on this principle. With this caveat, these results suggest that—given judicious emitter placement—one may indeed exploit this structure simultaneously to increase the decay rate of emitters and to couple their emission efficiently into a well-defined, specific guided-mode channel. The significant overlap of this mode with the SOI waveguide mode shown on the right of Fig. 1 can be used to ensure efficient coupling to a single low-loss dielectric waveguide mode and enable a very power-efficient source. For instance, if the MDSD structure shown in Fig. 3b is abruptly coupled to the equivalent SOI waveguide (i.e., the same structure with the metal and oxide layers removed, as on the right side of Fig. 1), the power transmittance between lowest-order TM modes is $\sim$85% at 850 nm, considering the propagation constant mismatch and mode overlap, and neglecting scattering into radiation modes.

Returning to the semi-infinite cases, we plot in Fig. 4a a comparison of the overall decay rate enhancement, $\hat{\gamma}$, with respect to a dipole in an infinite dielectric, for the MDS, MDM, and DM structures. Although this enhancement is strongest at the Ag–SiO_2 surface plasmon resonance ($\lambda_0 \approx 370$ nm), the MDS case exhibits a strong non-resonant enhancement of $\sim$40–60 between 600 and 1800 nm—only a factor of 2–3 smaller than that of the MDM structure; this behavior

#102844 - $15.00 USD Received 16 Oct 2008; revised 19 Dec 2008; accepted 22 Dec 2008; published 24 Dec 2008
(C) 2009 OSA

is nearly absent in the single-interface (DM) configuration. In particular, the enhancement at 1.5 μm is $\sim$60, suggesting that this effect could be particularly useful for Er^{3+}, which emits at this important telecommunications wavelength. It is important to note, however, that the enhancement decreases strongly with increased dielectric layer thickness [10], limiting the benefit of this effect in thicker Er-containing MOS structures such as those reported in [11] and [12].

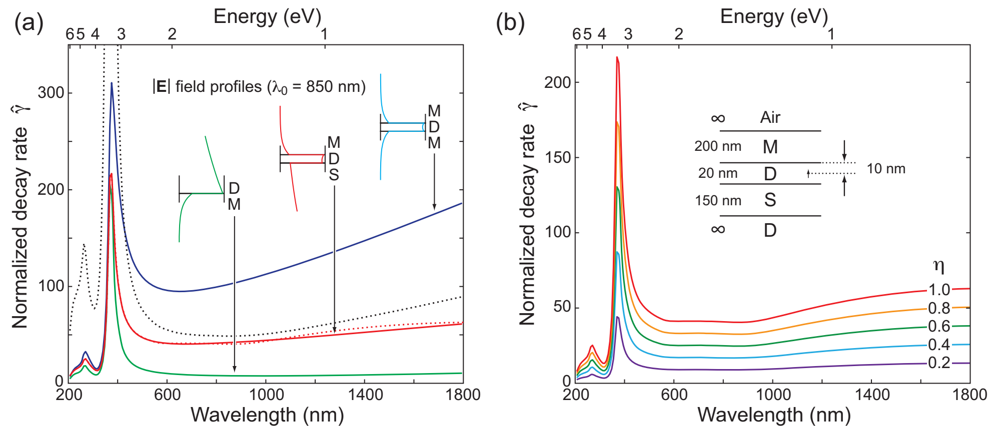

Fig. 4. (a) Decay rate enhancements for DM, MDS, and MDM structures; for these three cases, the dipole is 10 nm from the metal surface. Two plots for the MDSD case of Fig. 3b are included for comparison: (red dashed line) perpendicular dipole at the center of the dielectric ($d_+ = 10$ nm); (black dashed line) emitters uniformly distributed such that $d_+ \in [1.5, 18.5]$ nm in the dielectric layer, averaged over all dipole orientations. Insets: **E**-field profiles for $\lambda_0 = 850$ nm. (b) The effect of internal quantum efficiency (η) on the decay rate enhancement for the MDSD structure shown in the inset (perpendicular dipole, $d_+ = 10$ nm).

The behavior of the finite MDSD case (schematized in the inset to Fig. 3b) is also included in Fig. 4a for comparison with the three semi-infinite cases. The red dashed line is for the situation which most closely resembles the corresponding MDS case: a perpendicular dipole located at the center of the dielectric ($d_+ = 10$ nm). It is notable that, although the decay rate density spectra for the MDSD and MDS cases differ considerably due to the possibility of coupling to a well-defined hybrid SPP/Si-waveguide-like mode in the former (cf. Figs. 3a and 3b), the overall spontaneous emission rate enhancements for the two structures are very similar. The black dashed line describes a device which would more likely be produced by a typical fabrication scheme: a finite MDSD structure (layer thicknesses as shown in Fig. 3b) with randomly-oriented, uniformly-excited emitters distributed throughout a region of the dielectric layer ($d_+ \in [1.5, 18.5]$ nm), rather than being confined to a plane at the center. This situation would more realistically model a device using, for example, Si nanocrystals (NCs) formed via ion implantation for the emitters. Although the SP resonance peak at $\sim$370 nm is much higher than the case with dipoles at the dielectric center (due to the presence of emitters very close to the metal surface), the behavior in the non-resonant regime is comparable. It should be borne in mind that the fraction of power coupled into the useful SPP guided mode is a strong function of the dipole position (see the inset to Fig. 3b). As a result, the averaged enhancement shown in the black dashed plot is only representative of the *overall* decay rate in the ensemble and not specifically that of the SPP mode emission. The emitters closest to the metal would have the most rapid decay rate, but this power is inaccessible since it is lost to absorptive quenching processes. On the other hand, while the emitters which are closer to

#102844 - $15.00 USD Received 16 Oct 2008; revised 19 Dec 2008; accepted 22 Dec 2008; published 24 Dec 2008
(C) 2009 OSA

the oxide–silicon interface would not experience as high decay rates, they would couple most strongly to the useful guided mode.

So far, we have considered ideal emitters with unit internal quantum efficiency ($\eta = 1$). In practice, however, this is rarely the case; continuing with the foregoing example, well-passivated Si NCs can have $\eta \approx 0.6$ [19]. In Fig. 4b, for perpendicular dipoles at the center of the dielectric in the finite MDSD structure shown in the inset, we consider the effect of the emitters' internal quantum efficiency on the decay rate enhancement: a reduction in the quantum efficiency yields essentially a linear reduction in the decay rate enhancement for the wavelength range shown. From this result, we see that even for non-ideal emitters, a strong non-resonant enhancement in the decay rate is possible, further suggesting the viability of this architecture for an on-chip light source.

From an integrated photonics perspective, it is also important to consider the behavior of a MDS structure containing only standard materials used in integrated microelectronics fabrication processes; fortuitously, replacing the semi-infinite silver layer with CMOS-compatible aluminum yields very similar results. For a MDSD structure in analogy to Fig. 3b, approximately 79% of the emission at 1535 nm is coupled into the hybrid plasmonic/dielectric guided mode discussed previously. Furthermore, $\hat{\gamma}$ ranges from $\sim$25 to 55 between 600 and 1800 nm, achieving a value of 50 at 1.5 μm. We therefore suggest that, despite its somewhat greater absorptive loss in the visible and near infrared, Al may also be used to obtain similar, substantial enhancements in emission rate across a broad wavelength range. Although this paper focuses on the optical characteristics of the emitters, it is worth noting that careful design of the emitter-containing layer may be necessary to yield the efficient electroluminescence required for a viable integrated photonics component. For instance, improved charge injection through the dielectric layer would be possible if silicon nitride rather than silicon dioxide is used for the dielectric layer [20]. Using a higher-index dielectric would have the effect of reducing the overall enhancement somewhat due to the smaller dielectric contrast between the layers.

4. Conclusion

We have investigated spontaneous emission enhancements in planar MOS structures by considering the response of a semiclassical oscillating dipole at the center of a 20-nm-thick silica layer clad by semi-infinite Ag and Si layers. The decay rate density for TM modes is dominated by leaky radiation modes into the Si substrate, with additional absorptive loss at high $k_{\parallel}$ due to the proximity of the metal. The simulations predict radiative decay rate enhancements of 40 to 60 over a broad wavelength range (600 to 1800 nm) away from the Ag–SiO_2 surface plasmon resonance. Similar behavior is observed for finite-thickness metal–oxide–silicon–oxide structures. This enables strong preferential coupling into a single, well-defined waveguide mode, suggesting a viable pathway toward a new class of power-efficient, monolithically-integrated, CMOS-compatible light sources for all-silicon optoelectronics applications.

Acknowledgements

The authors thank Edward S. Barnard and Rohan D. Kekatpure for helpful discussions. A.C.H. gratefully acknowledges postdoctoral fellowship support from the Natural Sciences and Engineering Research Council of Canada (NSERC). This work was sponsored by the Si-based Laser Initiative of the Multidisciplinary University Research Initiative (MURI) under the Air Force Aerospace Research OSR Award Number FA9550-06-1-0470 and supervised by LTC Gernot Pomrenke.

#102844 - $15.00 USD Received 16 Oct 2008; revised 19 Dec 2008; accepted 22 Dec 2008; published 24 Dec 2008
(C) 2009 OSA